SOLAR CELLS

Organic and solution-processed tandem solar cells with 17.3% efficiency

Lingxian Meng[1], Yamin Zhang[1], Xiangjian Wan[1]*, Chenxi Li[1], Xin Zhang[1], Yanbo Wang[1], Xin Ke[1], Zuo Xiao[2], Liming Ding[2]*, Ruoxi Xia[3], Hin-Lap Yip[3], Yong Cao[3], Yongsheng Chen[1]*

Although organic photovoltaic (OPV) cells have many advantages, their performance still lags far behind that of other photovoltaic platforms. A fundamental reason for their low performance is the low charge mobility of organic materials, leading to a limit on the active-layer thickness and efficient light absorption. In this work, guided by a semi-empirical model analysis and using the tandem cell strategy to overcome such issues, and taking advantage of the high diversity and easily tunable band structure of organic materials, a record and certified 17.29% power conversion efficiency for a two-terminal monolithic solution-processed tandem OPV is achieved.

Organic photovoltaics (OPV) is considered to be a promising choice for next-generation technology platforms to address the increasing demands for renewable energy, owing to its many advantages such as low cost, flexibility, and large-area printing production (*1*–*3*). Indeed, there has been substantial improvement in the performance of OPV cells in the past decade, and the record power conversion efficiency (PCE) has been raised from ~5% to a current value of 14% (*3*, *4*). However, the performance of OPV cells still lags far behind that of other photovoltaic platforms based mainly on inorganic materials (*2*, *5*, *6*). This has led to the impression that OPV cells have a lower performance limit than inorganic material–based devices. A fundamental reason for this is the low charge mobility of organic materials (*7*, *8*), which limits the active-layer thickness of the devices and efficient sunlight absorption.

The tandem cell strategy is an effective way to simultaneously address these issues for OPV cells (*9*, *10*), and furthermore, is probably well suited for OPV (*11*–*15*). First, the use of tandem cells would overcome the thickness constraint of single-junction cells due to the low mobility of organic materials because wide and efficient absorption could be achieved by stacking the active layers with complementary absorption in tandem cells. Moreover, tandem cells can take advantage of one of the most important features of organic materials, i.e., their great diversity (*16*, *17*). This is because in tandem cells, active organic materials in each subcell require different but matching band structures, and such materials could in principle be designed and obtained owing to the high diversity, easily tunable band structures, and advanced synthesis of currently available organic materials (*18*). In addition, benefiting from this, the thermalization and transmission loss can be reduced in the tandem cells (*19*). Indeed, tandem cells have also been pursued widely for OPV, and ~14% PCE has been achieved (*11*), which is about the same as that obtained for the record single-junction cell (*4*). The limited performance of organic tandem cells is primarily due to their limited sunlight absorption range owing to the lack of optimal low-bandgap materials for use in the rear subcell, as most such materials can only absorb photons with an energy of ~1.3 eV (~900 nm) (*11*, *14*, *20*) and thus are missing a large part of the entire sunlight spectrum absorption. Another important reason is the limited tandem cell current owing to the absorption overlapping and/or current mismatching of subcells. With the above analysis and guided by a semi-empirical analysis, we report a solution-processed two-terminal (2T) monolithic tandem OPV cell with a new record PCE of 17.36%.

On the basis of previous theoretical work (*9*, *21*, *22*) and state-of-the art experimental results (*3*, *11*, *14*), we first have carried out a semi-empirical analysis for the possible but realistic PCE limit of 2T tandem OPV cells under Air Mass 1.5 Global (AM 1.5G) (details are provided in the supplementary materials and figs. S1 to S3). Briefly, in this model analysis, above the basic assumption for the Shockley-Queisser (SQ) limit analysis (*21*), the achievable PCEs (= $J_{sc} \times V_{oc} \times FF/P_{in}$, where J_{sc} is the short-circuit current density, V_{oc} is the open-circuit voltage, *FF* is the fill factor, and P_{in} is the power density of the incident light) are obtained using the following approaches: (i) the J_{sc} is assumed to be half of the theoretical current in the entire absorption range multiplied by a given external quantum efficiency (EQE) value; (ii) the V_{oc} is the sum of each subcell's voltage, while the voltage of each subcell is determined by the equation $eV_{oc} = E_g - E_{loss}$, where E_g (=1240/λ_{onset}) is the optical energy gap of the active layers (*23*), E_{loss} is the energy loss, e is the elementary charge, and λ_{onset} is the absorption onset of the active layers; (iii) the *FF* is assumed to be the state-of-the-art value. Based on these considerations, figs. S2 and S3 give the predicted achievable PCEs of 2T tandem cells for absorption onset (λ_{onset}) from 900 to 1200 nm, EQE in the range of 65 to 85%, E_{loss} in the range of 0.4 to 0.8 eV, and *FF* in the range of 0.65 to 0.80. These ranges represent the most likely achievable ones based on the state-of-the-art results (*3*, *4*, *24*–*27*), particularly when considering the wide diversity of organic/polymeric materials, including the recent development of small molecules/oligomer acceptor-donor-acceptor (A-D-A)–type donors (*14*, *28*, *29*) and acceptors (*3*, *16*). Extracted from these model results and as one example, Fig. 1A shows the achievable PCEs (14 to 28%) of the 2T tandem cells versus λ_{onset} (corresponding to E_g) of the rear-cell active layer, E_{loss}, and EQE, at a fixed *FF* of 0.75. Furthermore, as shown in Fig. 1B, a PCE of ~20% could be achieved if the $\lambda_{onset,\ rear\ cell}$ is ≤1100 nm with an average EQE of 75%, a *FF* of 0.75, and a typical E_{loss} of 0.6 eV, which is consistent with other theoretical analysis (*16*). From the model results shown in Fig. 1, C and D, and fig. S3, E_{loss} seems to have a bigger impact on the PCEs. Also, with E_{loss} increasing, the absorption onset of the rear cell ($\lambda_{onset,\ rear\ cell}$) with the maximum PCE has a tendency to blue-shift (Fig. 1, C and D) (details in the supplementary materials). These modeling results also indicate that the optimum $\lambda_{onset,\ rear\ cell}$, i.e., the E_g of the rear subcell active layer, is somewhat smaller than the optimum one from the SQ limit studies (of ~1127 nm) (*9*), probably owing to the large E_{loss} of OPV (*30*).

On the basis of the model analysis presented above, we discuss the screening of materials for use in tandem solar cells. For high-performance 2T tandem cells, various materials with wide and suitable bandgaps have been chosen for use in the front subcell (*16*). Critically, the first step is to choose suitable or optimal rear-subcell active materials with an infrared absorption onset up to 1050 to 1150 nm, based on the results shown in Fig. 1, B and C. This seemingly straightforward task has actually proved challenging, as a review of the literature (*10*, *20*) and our previous work (*14*) indicates that donor materials reported to date with absorption onset around 1100 nm essentially all suffer from large E_{loss}, and only a few showed high J_{sc} suitable for rear cells (*10*). Adding to this challenge is that the performance of these materials should also have an optimal *FF* and EQE in their single-junction cell evaluation. Fortunately, recent emerging nonfullerene molecules offer another optimal choice of rear-cell active materials owing to the widely tunable band

[1]State Key Laboratory and Institute of Elemento-Organic Chemistry, Centre of Nanoscale Science and Technology and Key Laboratory of Functional Polymer Materials, College of Chemistry, Nankai University, Tianjin, 300071, China. [2]Center for Excellence in Nanoscience (CAS), Key Laboratory of Nanosystem and Hierarchical Fabrication (CAS), National Center for Nanoscience and Technology, Beijing 100190, China. [3]Institute of Polymer Optoelectronic Materials and Devices, State Key Laboratory of Luminescent Materials and Devices, South China University of Technology, Guangzhou, 510640, China.
***Corresponding author. Email: yschen99@nankai.edu.cn (Y.C.); xjwan@nankai.edu.cn (X.W.); ding@nanoctr.cn (L.D.)**

structure of these A-D-A structures (*3*, *16*). After careful evaluation, we have found that the non-fullerene acceptor molecule CO_i8DFIC (also called O6T-4F, Fig. 2A) roughly meets these requirements (*4*, *31*), as it has an infrared absorption onset of ~1050 nm (optical bandgap E_g 1.20 eV) and, when blended with PTB7-Th as donor and $PC_{71}BM$ as the secondary acceptor (Fig. 2A and B) (*4*), a single-junction device based on it exhibited a high J_{sc} with an EQE >70% in the infrared absorption range, a *FF* of 69.7%, and a low E_{loss} of 0.51 eV.

Following the choice of rear-cell material, the next step is to find matching front subcell materials. From the above analysis, the maximum current achievable up to 1050 nm is ~31 mA/cm^2, assuming an EQE of 75% (fig. S1). With the requirement that both subcells must have the same current governed by the Kirchhoff's law to achieve optimal performance for a 2T tandem cell (*22*), the predicted best current of such a tandem cell should be ~15.5 mA/cm^2. A simple check of the theoretical current versus wavelength plot (fig. S1) indicates that the absorption onset of the front cell should be at ~720 nm. On the basis of these analyses, the front-cell active layer was selected to use PBDB-T as the donor and F-M as the acceptor (Fig. 2A and figs. S4 to S7) (*32*), as this active-layer mixture exhibits not only an absorption onset close to 720 nm, but also an optimal current of ~16 mA/cm^2 and a high EQE (average ~70% in the range of 300 to 750 nm), *FF* (69.8%), etc. in their single-junction device evaluation discussed below.

The performance of the each subcell was first studied and optimized using the inverted structures (see supplementary materials for details). The current density–voltage (*J-V*) curves of the optimized single-junction devices are shown in Fig. 2C, with the performance parameters detailed in table S1. The single-junction device for the front cell based on the selected active material of PBDB-T:F-M has a high EQE response in the range of 300 to 750 nm (Fig. 2D), giving a current of 15.96 mA/cm^2, together with a high V_{oc} of ~0.94 V and a *FF* of 69.8%. The performance of this inverted device is slightly different from that of the regular device (*32*), and the E_{loss} for this single-junction cell is 0.71 eV. The optimal J_{sc} is close to the value predicted for the front subcell required in the best tandem cell (details in tables S2 to S6). However, the optimized single-junction devices using PTB7-Th:O6T-4F:$PC_{71}BM$ for the rear unit gave a high current of 27.98 mA/cm^2 in the range from 300 to 1050 nm with a V_{oc} of 0.69 V, a *FF* of 69.7%, and a rather low E_{loss} of 0.51 eV, similar to that seen in the literature (*4*). Although the device showed a broad EQE response from 300 to 1050 nm (Fig. 2D), it has an integrated current of only 11.2 mA/cm^2 in the range of 720 to 1050 nm desired for the rear cell, lower than the best required current of 15.5 mA/cm^2 predicted above assuming a clear cut-off absorption for the rear subunit at 720 nm. The single-junction device using the pair of PTB7-Th:O6T-4F without $PC_{71}BM$

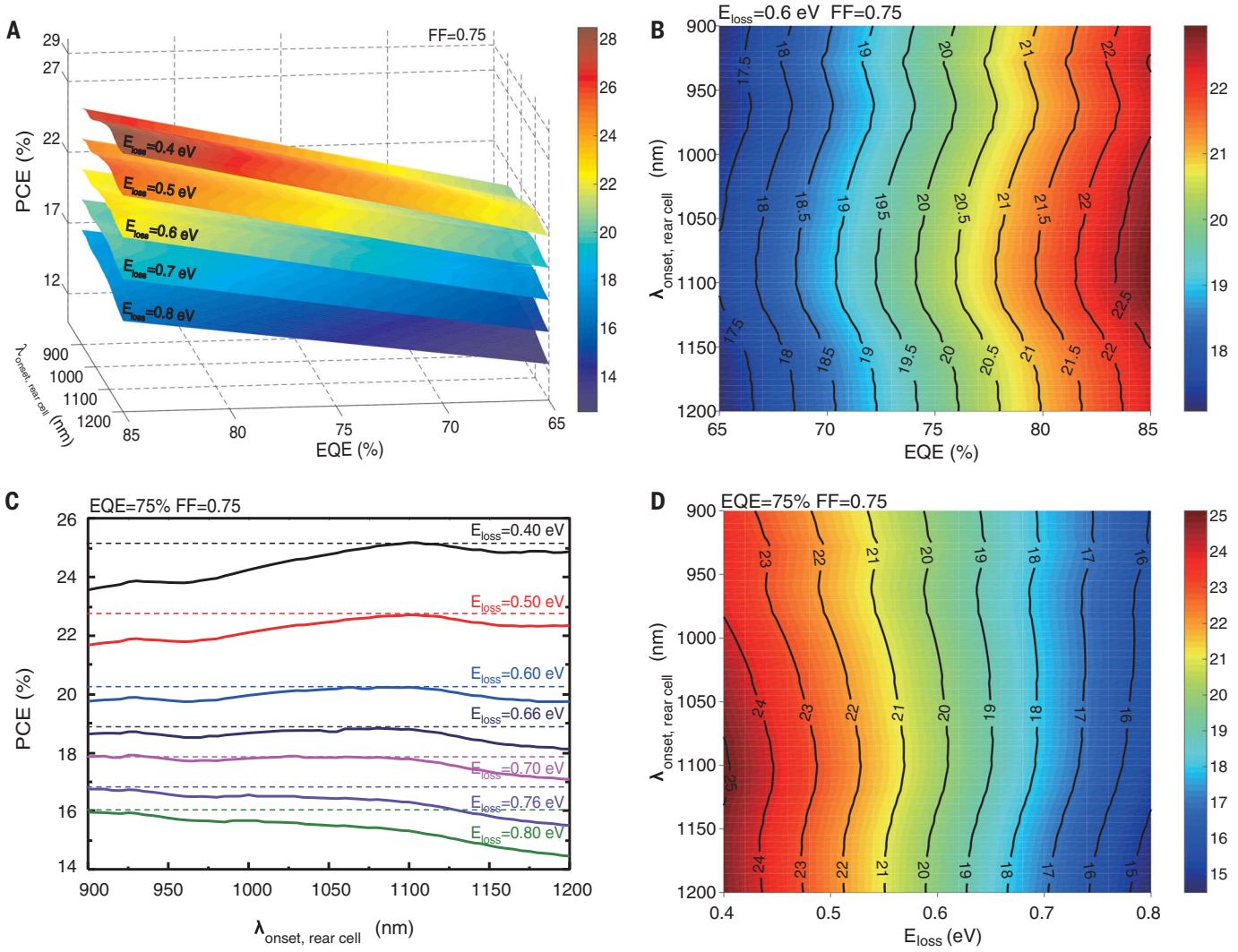

Fig. 1. Predicted PCEs of 2T tandem solar cells based on semi-empirical analysis under AM 1.5G. (**A**) PCEs versus EQE and $\lambda_{onset,\ rear\ cell}$, assuming E_{loss} of each subcell in the range of 0.4 to 0.8 eV and a fixed *FF* of 0.75. (**B**) PCEs versus EQE and $\lambda_{onset,\ rear\ cell}$, assuming E_{loss} of 0.6 eV and *FF* of 0.75. (**C**) PCEs versus $\lambda_{onset,\ rear\ cell}$ with E_{loss} of 0.4, 0.5, 0.6, 0.66, 0.7, 0.76, and 0.8 eV, *FF* of 0.75, and EQE of 75%. (**D**) PCEs versus E_{loss} and $\lambda_{onset,\ rear\ cell}$ with assumed EQE of 75% and *FF* of 0.75.

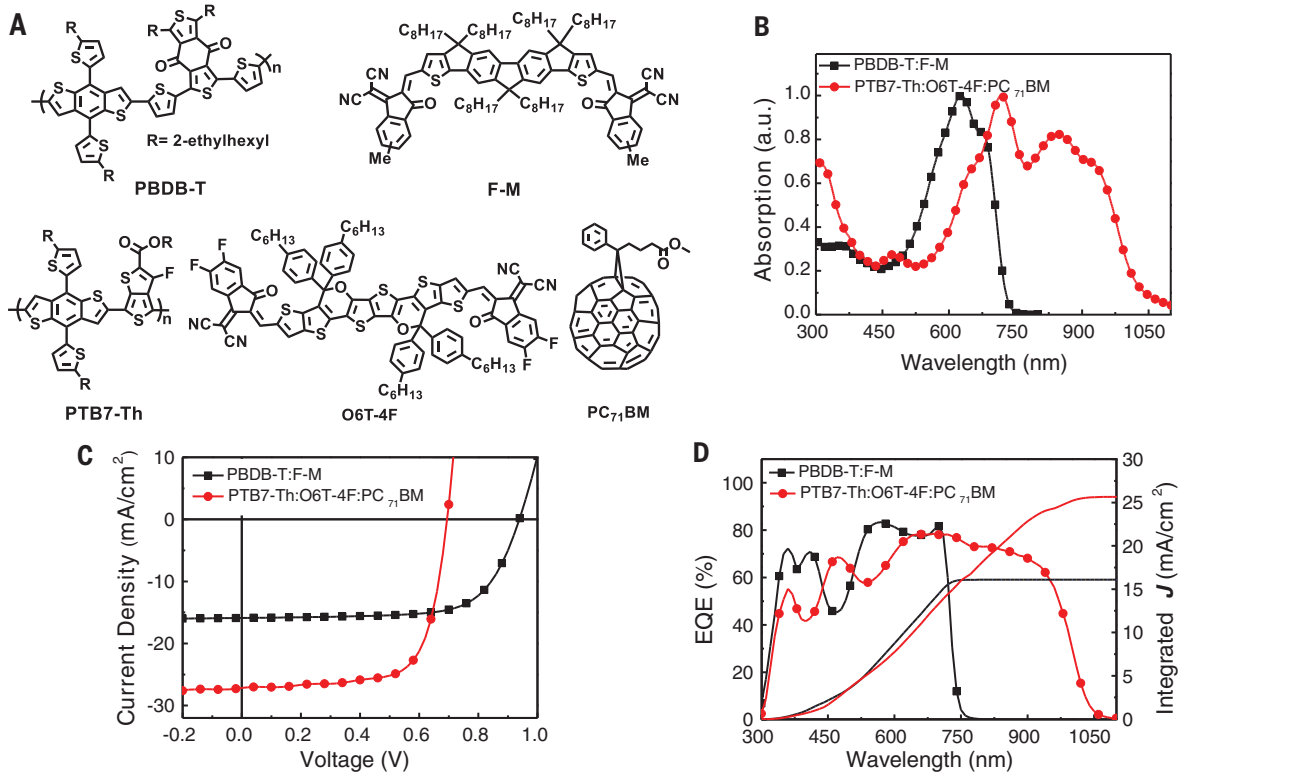

Fig. 2. Molecular structures and photovoltaic performance of the single-junction devices. (**A**) Molecular structures of PBDB-T, F-M, PTB7-Th, O6T-4F, and $PC_{71}BM$. (**B**) Normalized absorption spectra of PBDB-T:F-M and PTB7-Th:O6T-4F:$PC_{71}BM$ films. (**C**) *J-V* curves and (**D**) EQE curves of the single-junction devices based on PBDB-T:F-M and PTB7-Th:O6T-4F:$PC_{71}BM$ with an architecture of ITO/ZnO/PFN-Br/active layer/M-PEDOT/Ag and ITO/ZnO/ active layer/ MoO_3/Ag.

was also tested, but it gave an even lower current (*31*), as discussed below and in table S1.

After subcell optimization, the inverted tandem cells were fabricated using solution processing, and the detailed optimal results are shown in tables S7 to S13. The tandem cell architecture and corresponding energy diagram are presented in Fig. 3, A and B.

Before the tandem cell optimization, optical simulation modeling using the transfer matrix method (*33*) was conducted to develop guidelines for the selection of optimal thicknesses of the subcells, because one of the biggest challenges in fabricating efficient 2T tandem cells is obtaining a high balanced J_{sc}. Figure 3C displays the simulation results of the dependence of tandem cell J_{sc} versus the thicknesses of the two active layers. On the basis of the optical simulation, the best J_{sc} would be achieved with thicknesses of the optimized front and rear subcell active layers of ~200 and ~120 nm, respectively. The detailed photovoltaic results for difference thicknesses of subcells are summarized in Table 1 and fig. S8 and discussed in the supplementary materials. The tandem cells all showed a V_{oc} of ~1.64 V, approximately equal to the sum of the individual V_{oc}'s of the subcells, indicating an optimal interconnecting layer with good ohmic contact (*20*), whereas the J_{sc} and *FF* depended on the thickness of the subcells. Overall, the devices all showed excellent performance with PCEs above 15%. As shown in Fig. 3D and Table 1, the optimized 2T tandem cells gave a PCE of 17.36%, with a V_{oc} of 1.642 V, J_{sc} of 14.35 mA/cm^2, and *FF* of 73.7%, verified by the National Center of Supervision and Inspection on Solar Photovoltaic Products Quality of China (CPVT) with a measured PCE value of 17.29% (fig. S9). It is worth noting that the optimized tandem cell performance is well reproduced with a standard deviation (SD) of 0.29% of PCEs based on >50 devices with an average value of 16.89%, which is close to the best result (17.36%) (fig. S10).

The EQE of the tandem cell was measured following the protocol proposed in (*34*), and the results (Fig. 3E) show high values with an average of 72% in the absorption range from 300 to 1000 nm. The front cell showed a high EQE response in the range of 300 to 720 nm with a maximum EQE value of 76% at ~ 560 nm. The rear subcell absorbs mainly the low-energy photons (from ~720 to 1050 nm) with a strong EQE response of ~70% in the range of 740 to 940 nm, and the rear cell gave an integrated J_{sc} of 14.19 mA/cm^2, which closely matches the integrated J_{sc} (14.20 mA/cm^2) of the front cell. The high and balanced J_{sc} of the two subcells is attributed to their complementary absorptions and high-efficiency photoresponse. The tandem cells without the secondary acceptor $PC_{71}BM$ in the rear cell were also studied but gave PCEs below 16%, owing to the relatively low current and *FF*, which is probably caused by the weaker absorption and lower EQE values in the range of 900 to 1050 nm (fig. S11). This is consistent with earlier results (*4*, *31*) and probably due to the morphology difference in the active layer caused by adding $PC_{71}BM$ (see details in the supplementary materials).

The optimal J_{sc} obtained was ~14.3 mA/cm^2, which is still less than 15.5 mA/cm^2 predicted for the best tandem cell with absorption onset up to 1050 nm. Clearly, an important reason for this is the effective absorption of only up to ~985 nm (Fig. 3E) versus the required best absorption of 1050 nm. Also the average (~72%) EQE is still lower than the 75% used in the analysis shown in Fig. 1B. Furthermore, the V_{oc} obtained for our tandem cell is ~1.64 V and nearly equal to the sum of the V_{oc}'s of the two subcells. However, it represents 73% of the theoretical value (*35*), corresponding to a substantial E_{loss} (0.71 and 0.51eV, or an average of 0.61 eV) of the front and rear cells, respectively. Together with recent results showing E_{loss} for some OPV cells as small as 0.45 eV E_{loss} (*26*), considerable improvement is expected for reducing E_{loss} through methods such as morphological or interfacial engineering in addition to the optimization of materials (*36*–*39*). Considering the bigger impact of E_{loss} on the overall performance as discussed previously (*23*, *30*), reducing E_{loss} should be a focus of future work. The tandem cell *FF* in this work is as high as 74%, also slightly higher than that of the

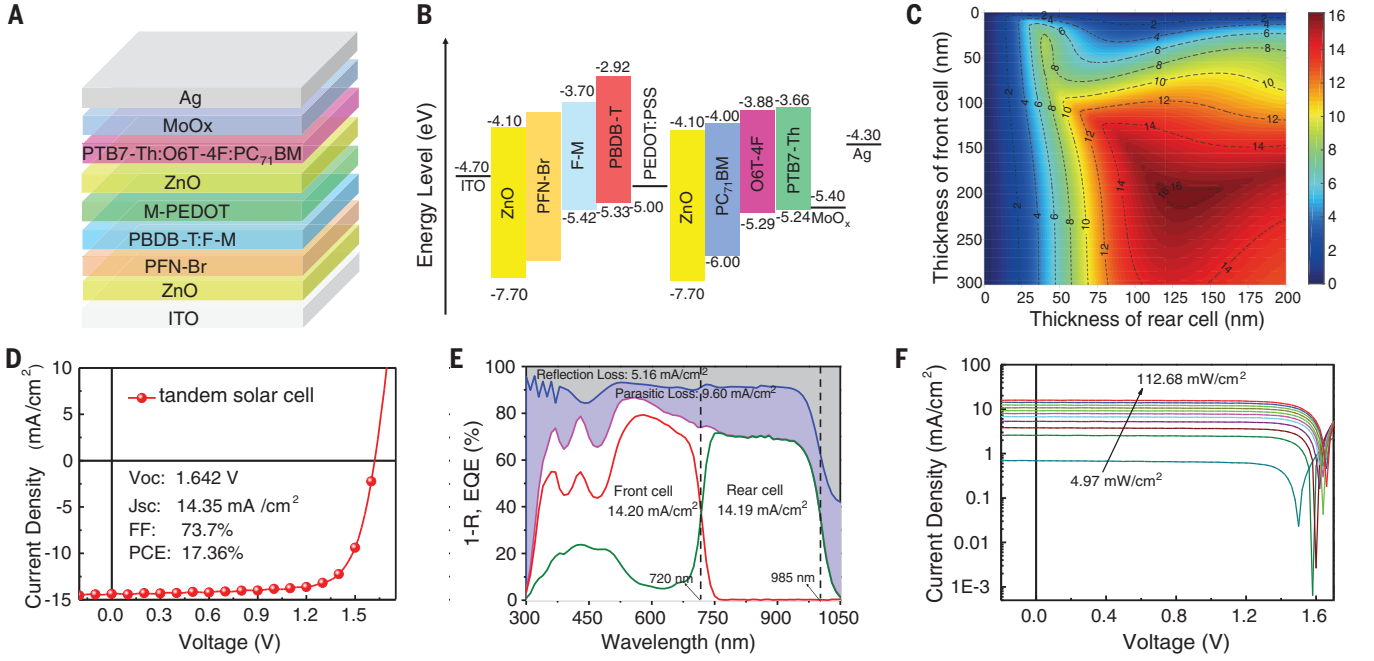

Fig. 3. Optical simulation and photovoltaic performance of the tandem cells. (**A**) Device architecture of the tandem cell. (**B**) Energy level diagram of the tandem solar cell. (**C**) Simulated current density generated in a tandem cell as a function of the thicknesses of the active layers. (**D**) *J-V* curve. (**E**) EQE and 1-reflectance (1-R) of the optimized tandem solar cell and (**F**) *J-V* curve of the tandem cells under different light intensities, ranging from 4.97 to 112.68 mW/cm^2. The dashed vertical line at 720 nm in (E) is the cross point of the EQE plots of the two subcells, and the dashed vertical line at 985 nm indicates the effective absorption up position (assuming 50% EQE) of the rear subcell.

Table 1. 2T tandem cell performance with different thicknesses of the subcells. Results are shown as the mean ± SD. Values in parentheses denote the best optimal results.

Thickness (nm)		V_{oc} (V)	J_{sc} (mA/cm^2)	*FF* (%)	PCE (%)
Front cell	Rear cell				
120	110	1.646 ± 0.008 (1.646)	13.11 ± 0.23(13.32)	73.0 ± 0.6(73.2)	15.75 ± 0.03(16.05)*
135	110	1.634 ± 0.005(1.645)	13.76 ± 0.27(13.85)	71.2 ± 1.1(71.6)	16.01 ± 0.35(16.31)*
150	**110**	**1.636 ± 0.014(1.642)**	**14.32 ± 0.18(14.35)**	**72.1 ± 1.4(73.7)**	**16.89 ± 0.29(17.36)†**
165	110	1.630 ± 0.012(1.644)	14.21 ± 0.18(14.37)	68.3 ± 1.2(69.1)	15.82 ± 0.29(16.32)*
180	110	1.631 ± 0.010(1.636)	14.14 ± 0.25(14.34)	64.9 ± 1.2(65.9)	14.97 ± 0.32(15.46)*
150	125	1.635 ± 0.007(1.626)	14.08 ± 0.21(14.19)	69.9 ± 1.1(70.1)	16.09 ± 0.20(16.17)*
150	90	1.630 ± 0.010(1.636)	14.03 ± 0.28(14.00)	69.1 ± 0.8(69.6)	15.80 ± 0.22(15.94)*

*The average parameters were calculated from more than 20 devices. †The average parameters were calculated from 84 devices, and the area of the devices studied under the optimization condition is ~4 mm^2.

two subcells with a *FF* of ~70%, indicating that the reduced charge recombination in the tandem cell suppressed the carrier dynamics loss (*19*), but still lower than the best FF (80%) achieved (*25*) and theoretical values (85 to 94%) for devices with a bandgap between 1.0 and 3.0 eV (*35*).

The performance of the optimized tandem cells was also measured under different illumination intensities, from 0.05 to 1.12 sun (Fig. 3F and fig. S12). The PCEs of the tandem cells remain above 15% when the light intensity varies from 4.97 to 112.68 mW/cm^2, and a PCE of 17.87% has been achieved at a light intensity of 25.99 mW/cm^2. In addition, the tandem cells show good stability behavior, with only a minor performance degradation of 4% after continuous testing for 166 days (fig. S13). Furthermore, we also fabricated tandem cells with large areas, and the preliminary results (table S14) show good performance even at sizes up to 100 mm^2.

The much better PCE of 17.36% compared with current state-of-the-art levels, together with the semi-empirical analysis provided, indicate that OPV tandem cells have a greater potential than previously thought, and a PCE >25% should be attainable with the already achieved best EQE of 80% (*3*), E_{loss} of 0.45 eV (*26*), and *FF* of 0.75 (*25*). Considering its other advantages, OPV should be competitive with other solar cell technologies for industry applications in the future if the issue of OPV stability can be addressed.

REFERENCES AND NOTES

1. M. C. Scharber, N. S. Sariciftci, *Prog. Polym. Sci.* **38**, 1929–1940 (2013).
2. A. Polman, M. Knight, E. C. Garnett, B. Ehrler, W. C. Sinke, *Science* **352**, aad4424 (2016).
3. J. Hou, O. Inganäs, R. H. Friend, F. Gao, *Nat. Mater.* **17**, 119–128 (2018).
4. Z. Xiao, X. Jia, L. Ding, *Sci. Bull.* **62**, 1562–1564 (2017).
5. K. Yoshikawa *et al.*, *Nat. Energy* **2**, 17032 (2017).
6. W. S. Yang *et al.*, *Science* **348**, 1234–1237 (2015).
7. Q. Burlingame *et al.*, *Nature* **554**, 77–80 (2018).
8. U. Würfel, D. Neher, A. Spies, S. Albrecht, *Nat. Commun.* **6**, 6951 (2015).
9. A. D. Vos, *J. Phys. D Appl. Phys.* **13**, 839–846 (1980).
10. G. Li, W.-H. Chang, Y. Yang, *Nat. Rev. Mater.* **2**, 17043 (2017).
11. Y. Cui *et al.*, *J. Am. Chem. Soc.* **139**, 7302–7309 (2017).
12. W. Li, A. Furlan, K. H. Hendriks, M. M. Wienk, R. A. Janssen, *J. Am. Chem. Soc.* **135**, 5529–5532 (2013).
13. N. Li, C. J. Brabec, *Energy Environ. Sci.* **8**, 2902–2909 (2015).

14. M. Li *et al*., *Nat. Photonics* **11**, 85–90 (2017).
15. J. Y. Kim *et al*., *Science* **317**, 222–225 (2007).
16. P. Cheng, G. Li, X. Zhan, Y. Yang, *Nat. Photonics* **12**, 131–142 (2018).
17. Y. J. Cheng, S. H. Yang, C. S. Hsu, *Chem. Rev.* **109**, 5868–5923 (2009).
18. Z. B. Henson, K. Müllen, G. C. Bazan, *Nat. Chem.* **4**, 699–704 (2012).
19. L. Zuo *et al*., *Adv. Mater.* **30**, 1706816 (2018).
20. T. Ameri, N. Li, C. J. Brabec, *Energy Environ. Sci.* **6**, 2390–2413 (2013).
21. W. Shockley, H. J. Queisser, *J. Appl. Phys.* **32**, 510–519 (1961).
22. G. Dennler *et al*., *Adv. Mater.* **20**, 579–583 (2008).
23. S. Matthew Menke, A. Niva, *Joule* **2**, 25–35 (2018).
24. Z. He *et al*., *Nat. Photonics* **9**, 174–179 (2015).
25. X. Guo *et al*., *Nat. Photonics* **7**, 825–833 (2013).
26. Z. Yao *et al*., *J. Am. Chem. Soc.* **140**, 2054–2057 (2018).
27. J. Liu *et al*., *Nat. Energy* **1**, 16089 (2016).
28. Q. Zhang *et al*., *Nat. Photonics* **9**, 35–41 (2015).
29. Y. Chen, X. Wan, G. Long, *Acc. Chem. Res.* **46**, 2645–2655 (2013).
30. J. Benduhn *et al*., *Nat. Energy* **2**, 17053 (2017).
31. Z. Xiao *et al*., *Sci. Bull.* **62**, 1494–1496 (2017).
32. Y. Zhang *et al*., *Adv. Mater.* **30**, 1707508 (2018).
33. G. F. Burkhard, E. T. Hoke, M. D. McGehee, *Adv. Mater.* **22**, 3293–3297 (2010).
34. R. Timmreck *et al*., *Nat. Photonics* **9**, 478–479 (2015).
35. S. Rühle, *Sol. Energy* **130**, 139–147 (2016).
36. Y. Huang, E. J. Kramer, A. J. Heeger, G. C. Bazan, *Chem. Rev.* **114**, 7006–7043 (2014).
37. Z. A. Page, Y. Liu, V. V. Duzhko, T. P. Russell, T. Emrick, *Science* **346**, 441–444 (2014).
38. Z. Wu *et al*., *J. Am. Chem. Soc.* **138**, 2004–2013 (2016).
39. H. Bin *et al*., *Nat. Commun.* **7**, 13651 (2016).

ACKNOWLEDGMENTS

Funding: We gratefully acknowledge the financial support from MoST (2014CB643502, 2016YFA0200200, 2017YFA0206600), NSFC (51773095, 91633301) of China, and Tianjin City (17JCJQJC44500, 17JCZDJC31100). **Author contributions:** Y.C. and X.W. conceived and directed the study. L.M. fabricated and characterized the tandem cells, and Y.Z. fabricated and evaluated the single-junction devices. O6T-4F was provided by L.D. and Z.X.; X.Z. and Y.W. synthesized the other materials. R.X. and H.Y. carried out the *n*, *k* measurement, and X.K. carried out the simulation of the tandem cell with different subcell thicknesses. The manuscript was mainly prepared by Y.C., L.M., X.W., and C. L., and all authors participated in the manuscript preparation and commented on the manuscript. **Competing interests:** The authors declare no competing interests; **Data and materials availability:** All data are available and presented in the main text and the supplementary materials. We have applied for a patent for this work.

SUPPLEMENTARY MATERIALS

www.sciencemag.org/content/361/6407/1094/suppl/DC1
Materials and Methods
Figs. S1 to S13
Tables S1 to S14
References (*40*–*49*)

23 March 2018; accepted 25 June 2018
Published online 9 August 2018
10.1126/science.aat2612

Science

Organic and solution-processed tandem solar cells with 17.3% efficiency

Lingxian Meng, Yamin Zhang, Xiangjian Wan, Chenxi Li, Xin Zhang, Yanbo Wang, Xin Ke, Zuo Xiao, Liming Ding, Ruoxi Xia, Hin-Lap Yip, Yong Cao and Yongsheng Chen

Science **361** (6407), 1094-1098.
DOI: 10.1126/science.aat2612originally published online August 9, 2018

Tailoring tandem organics

Tandem solar cells can boost efficiency by using a wider range of the solar spectrum. The bandgap of organic semiconductors can be tuned over a wide range, but, for a two-terminal device that directly connects the cells, the currents produced must be nearly equal. Meng *et al.* used a semiempirical analysis to choose well-matched top- and bottom-cell active layers. They used solution processing to fabricate an inverted tandem device that has a power conversion efficiency as high as 17.4%.

Science, this issue p. 1094